On the role of UV crosslinking to enhance moderate-temperature operation of truly solid-state Li-metal batteries based on recycled-PVB-modified polyether electrolytes

Journal of Power Sources 662 (2026) 238704

Contents lists available at ScienceDirect

Journal of Power Sources

journal homepage: www.elsevier.com/locate/jpowsour

On the role of UV crosslinking to enhance moderate-temperature operation of truly solid-state Li-metal batteries based on recycled-PVB-modified polyether electrolytes

Leonardo Balducci [a,b,*], Hamideh Darjazi [a,b], Alessandro Piovano [a,b], Giuseppe Antonio Elia [a,b], Claudio Gerbaldi [a,b,**]

[a] GAME Lab, Department of Applied Science and Technology (DISAT), Politecnico di Torino, Corso Duca degli Abruzzi, 24, 10129, Torino, Italy
[b] National Reference Center for Electrochemical Energy Storage (GISEL) - INSTM, Via G. Giusti 9, Firenze, 50121, Italy

HIGHLIGHTS

- Solid polymer electrolytes by blending PEO with recycled PVB (re-PVB).
- Blends show enhanced ionic conductivity and mechanical stability.
- Strong synergistic effect by UV curing and polymer blending in PEO/re-PVB.
- Crosslinked PEO/re-PVB electrolytes with high performance at 40 °C.
- Stable cycling with both NMC811 and LFP cathodes.

GRAPHICAL ABSTRACT

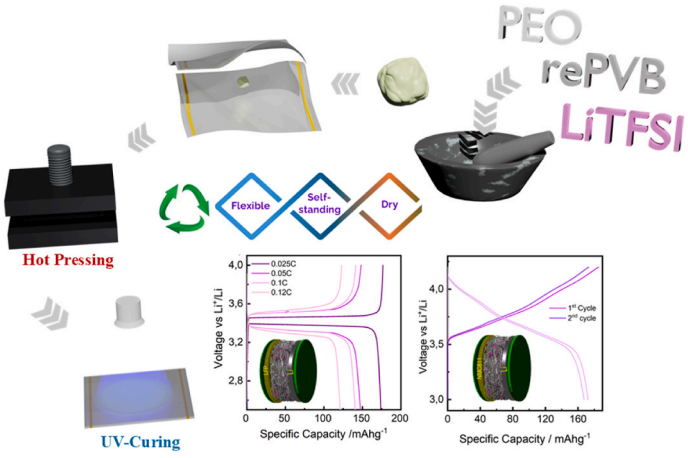

ARTICLE INFO

Keywords:
Solid-state battery
Crosslinking
Lithium battery
Solvent-free

ABSTRACT

Unleashing the potential of truly solid-state lithium metal batteries (SSLMBs) requires scalable, industrially viable manufacturing compatible with mild processing conditions. At the same time, promoting sustainable practices, such as material reuse and waste reduction, is essential for environmentally responsible, sustainable-by-design battery development. Herein, we report a flexible, self-standing, truly solid polymer electrolyte (SPE) fabricated via simple, solvent-free UV-induced crosslinking (UV-curing) process that supports moderate-temperature, large-scale manufacturing. The crosslinked polymer electrolyte combines poly(ethylene oxide)

This article is part of a special issue entitled: In memory of Professor Bruno Scrosati published in Journal of Power Sources.

* Corresponding author. GAME Lab, Department of Applied Science and Technology (DISAT), Politecnico di Torino, Corso Duca degli Abruzzi, 24, 10129, Torino, Italy.
** Corresponding author. GAME Lab, Department of Applied Science and Technology (DISAT), Politecnico di Torino, Corso Duca degli Abruzzi, 24, 10129, Torino, Italy.
E-mail addresses: leonardo.balducci@polito.it (L. Balducci), claudio.gerbaldi@polito.it (C. Gerbaldi).

https://doi.org/10.1016/j.jpowsour.2025.238704
Received 23 September 2025; Received in revised form 24 October 2025; Accepted 26 October 2025
Available online 10 November 2025

Polymer electrolyte
Recycling

(PEO), the ion-conductive phase, with recycled poly(vinyl butyral) (Re-PVB), a mechanically robust polymer derived from laminated glass waste. Electrochemical studies reveal that the UV-cured SPE has excellent compatibility with lithium metal, enabling stable lithium plating/stripping with low interfacial resistance at 40 °C. Moreover, laboratory-scale truly SSLMB cells with high-loading LFP catholyte (12 mg cm^{-2}) show remarkable performance with almost full specific capacity delivered at low C-rate and excellent rate capability. Noteworthy, promising performance is also obtained in Li-metal cells with high-loading NMC811 catholyte (7 mg cm^{-2}). Overall, this dual-modified SPE development strategy, combining UV-crosslinking and the use of recycled polymers, offers an energy-efficient and sustainable route toward high-performance solid polymer electrolytes, advancing the practical and eco-friendly development of next-generation SSLMBs.

1. Introduction

The shift toward a sustainable global economy increasingly relies on the adoption of low-carbon footprint, environmentally responsible development pathways. In response, numerous countries have embedded circular economy principles into national strategies to enhance resource efficiency, reduce environmental impact, and strengthen long-term economic resilience [1].

In this broader sustainability framework, the lithium battery industry has identified the circular economy as a key enabler of environmentally sound and resource-efficient production. This involves integrating upcycled and/or recycled materials into the supply chain and minimizing waste generation, thereby supporting the development of more robust and sustainable battery systems [2–4].

While significantly enhancing the specific capacity of cathode and anode materials remains a challenge, improvements in energy density may be more effectively realized through innovations in electrolyte design. Additionally, enhancing safety has become critical, particularly by replacing flammable organic solvent-based liquid electrolytes with safer alternatives.

In this context, the emergence of solid-state electrolytes (SSEs) offers a promising solution to these challenges [5]. SSEs also enable the practical implementation of lithium metal anodes, which are widely regarded as essential for next-generation batteries due to their exceptionally high theoretical capacity (3860 mAh g^{-1}) and the lowest electrochemical potential (−3.04 V *vs.* SHE). Unlike conventional liquid systems, where lithium metal suffers from continuous side reactions, dendrite formation, and unstable solid electrolyte interphase (SEI) development, SSEs provide a more stable interfacial environment [6]. This stability facilitates the fabrication of lithium metal batteries (LMBs) with significantly enhanced energy density and improved safety characteristics.

Among various SSEs, solid-state polymer electrolytes (SPEs) have gained significant attention due to their excellent mechanical properties, favorable electrode compatibility, which reduces interfacial resistance, ease of film formation, and cost-effectiveness, making them promising for practical energy storage applications [7,8]. However, their relatively low ionic conductivity at ambient temperature remains a critical bottleneck hindering their widespread use [9]. To address the trade-off between ionic conductivity and mechanical strength, several strategies have been explored, including polymer grafting or blending [10], physical or chemical crosslinking [11–13], and the incorporation of organic fillers [14,15]. Among these, UV-induced crosslinking (UV-curing) is particularly appealing because it enables rapid formation of crosslinked polymer networks within minutes, enhancing both mechanical stability and ionic conductivity at a mild temperature [16,17]. Polymer blending offers a powerful route to improve structural robustness and electrochemical performance simultaneously; representative examples include poly(ethylene oxide) (PEO)-based systems such as PEO/poly(vinylidene fluoride) (PEO/PVDF) [18], PEO/poly(vinylpyrrolidone) (PEO/PVP) [19], PEO/poly(vinyl chloride) (PEO/PVC) [20], and PEO/poly(acrylonitrile) (PEO/PAN) [21].

In our previous work, guided by sustainability and circular economic principles, we developed a high-performance, PEO/recycled poly(vinyl butyral) (Re-PVB) blend electrolyte [22]. This is a truly solid-state salt-in-polymer electrolyte as no solvent(s) and/or plasticizer(s) were used/added either during materials preparation and/or cell operation. PVB, commonly employed as an interlayer in laminated glass due to its exceptional adhesion properties, optical transparency, and mechanical stiffness [22,23], offers distinct advantages when integrated into polymer electrolytes [24]. Specifically, blending with PEO strengthens interfacial interactions between the electrolyte and electrode, while its pendant functional groups promote the formation and retention of amorphous domains, thereby facilitating ionic transport [25,26]. Given that PVB constitutes a major waste stream following laminated glass disposal, its valorization directly supports circular economy initiatives, offering both environmental benefits and energy recovery potential [4] [27]. Nevertheless, conventional PVB recycling remains challenged by material impurities and scalability constraints. Addressing this need, the European "SUNRISE" project focuses on (i) the selective recovery of recyclable PVB fractions for reuse in their original applications, and (ii) the upcycling of non-recyclable fractions into high-value products, including functional materials for energy storage technologies.

In this context, here we propose a dual modification strategy for solid polymer electrolytes by combining the use of Re-PVB blended with PEO and of UV-curing to obtain a fully crosslinked network to synergistically improve properties of the final material. Particularly, this approach aims at improving mechanical robustness while concurrently enhancing the amorphous domains within the system, thereby boosting ionic conductivity at low temperatures. In addition, it aligns with circular economy principles by repurposing Re-PVB, a material that generates significant waste upon disposal, for sustainable and high-performance energy storage applications.

2. Experimental

Materials. Poly(ethylene oxide) – PEO (Mw = 4×10^5 g mol^{-1}, CAS 25322-68-3), lithium bis(trifluoromethanesulfonyl)imide (LiTFSI, battery grade, CAS 90076-65-6), 4,4′-difluorobenzophenone (99 %, CAS 345-92-6, used as a photoinitiator), deuterated dimethyl sulfoxide (d_6-DMSO, 99.5 % D, CAS 2206-27-1), ethyl acetate (EtOAc, CAS 141-78-6), and acetonitrile (ACN, CAS 75-05-8) were all obtained from Merck. Recycled poly(vinyl butyral) (namely, Re-PVB) was isolated from end-of-life laminated automotive glass through a proprietary mechanochemical process. Characterization of the recovered material showed a molecular weight of ~135,000 g mol^{-1}, a broad distribution of chain lengths, and residual plasticizer in a polymer-to-plasticizer mass ratio of roughly 1:1 [28]. Poly(vinylidene fluoride) – (PVDF, CAS 24937-79-9) was obtained from Solvay, while conductive carbon black (Super C65, CAS 1333-86-4), N-methyl-2-pyrrolidone (NMP, CAS 872-50-4), lithium nickel manganese cobalt oxide ($LiNi_{0.8}Mn_{0.1}Co_{0.1}O_2$, NMC811, CAS 346417-97-8), and lithium iron phosphate ($LiFePO_4$, LFP, CAS 15365-14-7) were supplied by Sigma-Aldrich. Before use, all materials were vacuum-dried and stored in an argon-filled glovebox (M-Braun Unilab) with O_2 and H_2O contents below 0.5 ppm.

UV curing, SSLMBs assembly and electrochemical testing. The UV-cured SPE was prepared according to the optimal composition identified in our previous study: PEO and LiTFSI in a 15:1 molar ratio (Li/EO) with

10 wt% Re-PVB. PEO and Re-PVB were first mechanically ground to break up Re-PVB agglomerates and obtain a uniform mixture. Subsequently, 4,4′-difluorobenzophenone (5 wt% relative to PEO) was incorporated as a type-II (hydrogen abstraction from aromatic ketones) UV photoinitiator and further ground to ensure even dispersion. LiTFSI was then added in the specified ratio and mixed manually until a cohesive composite dough was formed.

The blend was hot-pressed in two stages between polypropylene sheets, using Kapton tape (55 μm thickness) as a gasket: first at 70 °C under 1 bar for 5 min, followed by 70 °C under 10 bar for 5 min. The resulting solid-state electrolyte film was UV-cured on both sides for 5 min each with a xenon lamp (40 mW cm^{-2}) thus suppressing crystallization by creating a strong three-dimensional network (see Fig. 1). The UV-cured electrolyte was designated as **SPE-UV**, while the uncrosslinked reference (pristine) electrolyte was denoted **SPE-P**.

The SPE performance was evaluated in solid-state Li-metal cells configured as Li‖SPE-UV‖cathode. Assembly was housed in a EL-Cell Std (EL-CELL, Germany), and galvanostatic cycling was conducted at 40 °C. Two different cathode formulations were tested: an LFP-based composite and NMC811-based composite, each consisting of active material, Super C65, and a catholyte with the same composition as the PEO–LiTFSI electrolyte, combined in a 75:5:20 wt ratio. For coating, the slurries were applied to aluminum foil using a doctor blade with a 500 μm gap. All coated electrodes were dried under vacuum at 80 °C overnight. Rate of 1C corresponded to a specific current of 170 mA g^{-1} for LFP ($2.5 \leq E\ (V) \leq 4$) and 180 mA g^{-1} for NMC ($3 \leq E\ (V) \leq 4.2$), calculated based on the active material mass loading of 12 mg cm^{-2} for LFP and 7 mg cm^{-2} for NMC811. Electrochemical impedance spectroscopy (EIS) was carried out on the Li‖SPE-UV‖LFP full-cell configuration within the frequency range of 100 kHz to 100 mHz. Measurements were performed at 40 °C, both before cycling and after completion of the cycling tests. Different contributions to the overall cell impedance can be distinguished across the frequency spectrum: (i) the intercept with the real axis reflects the bulk resistance of the SPE layer (R_s), which is governed by both its ionic conductivity and thickness; (ii) two partially overlapping semicircles appearing in the high-to-intermediate frequency range are associated with interfacial resistances (R_{int}), which may arise from either ion-transfer or charge-transfer processes depending on the electrode/electrolyte interface; and (iii) at low frequencies, the characteristic inclined line represents the Warburg element (W), corresponding to the diffusion of Li^+ ions toward the blocking electrode.

(Electro)chemical Characterization. The gel content was determined to quantify the proportion of polymer chains that remained uncrosslinked after UV curing. Approximately 0.65 g of the material was enclosed in a 500-mesh metal container and immersed in 50 mL of ethyl acetate (EtOAc) for 1 h under stirring at room temperature. The solvent was then replaced with a fresh 50 mL portion of EtOAc, and the extraction continued for 24 h under the same conditions. A third extraction was carried out using another 50 mL of fresh EtOAc for 3 h. After extraction, the sample was recovered and dried in a vacuum oven until a constant weight was obtained. For statistical purposes, the extraction sequence with EtOAc was performed two additional times under identical conditions. Gel content was calculated according to Equation (1).

$$G\% = W_i / W_o \times 100 \quad (1)$$

where W_i is the final weight of the sample, and W_0 is the initial weight before treatment. To further verify the crosslinking efficiency, photorheology was conducted using an Anton Paar MCR 702e MultiDrive modular rheometer equipped with a UV lamp. The measurements were performed at 70 °C, with the UV lamp calibrated to deliver 40 mW cm^{-2} using a DMAX photometer.

Differential scanning calorimetry (DSC) analyses were performed using a Netzsch 214 Polyma instrument to determine the reduction of the system crystallinity. Measurements were conducted over a temperature range from −50 to +90 °C, with a heating rate of 10 °C min^{-1}, under a nitrogen flow of 40 mL min^{-1}. The degree of crystallinity was calculated according to Equation (2), adopting 205 J g^{-1} as the melting enthalpy (ΔHm^0) corresponding to 100 % crystalline PEO.

$$Cristallinity\% = \Delta H_m{}^i / \Delta H_m{}^o \times 100 \quad (2)$$

Thermogravimetric analysis (TGA) was carried out using a Netzsch TG 209 F3 instrument to assess the thermal stability of the samples. Measurements were performed from 25 to 800 °C under a nitrogen atmosphere, with a gas flow rate of 100 mL min^{-1} and a heating rate of 10 °C min^{-1}. The temperature corresponding to a 5 % weight loss (Td_5 %) was taken as the reference point for evaluating the onset of degradation.

Lithium plating/stripping tests were performed at 40 °C using a symmetric Li‖SPE-UV‖Li configuration in CR2032 coin cells. The cells were assembled in an argon-filled glovebox, employing 12 mm metallic Li electrodes and a 16 mm SPE membrane as the electrolyte. Cycling began at 0.025 mA cm^{-2} (fixed areal capacity: 0.20 mAh cm^{-2}) and increased stepwise to 0.050, 0.100, and 0.200 mA cm^{-2}. Then experiments were conducted at a fixed current regime of 0.025 mA cm^{-2} and were prolonged for a total duration of 650 h. EIS was carried out both before the start and after the completion of cycling to evaluate changes in the SPE internal resistance. Impedance data from the Nyquist plots

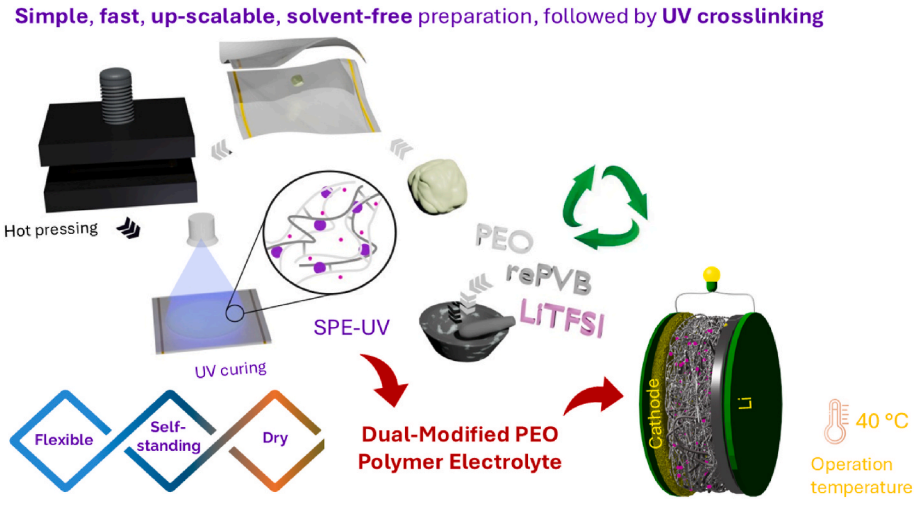

Fig. 1. Schematic illustration of the SPE-UV electrolyte preparation process.

were analyzed using an equivalent circuit approach, applying a non-linear least square (NLLS) fitting routine in RelaxIS3 (rhd instruments, Darmstadt, Germany). The circuit model adopted was $R_e(R_{int}C_{int})Q_w$, following Boukamp's notation. In this configuration, R_e corresponds to the bulk resistance of the SPE, while R_{int} and C_{int} describe the charge-transfer resistance and the double-layer capacitance at the electrode–electrolyte interface. The element Q_w represents the Warburg-type impedance linked to semi-infinite ion diffusion. For improved fitting accuracy, the ideal capacitive component (C_{int}) was replaced by a constant-phase element (Q), which accounts for non-ideal behavior arising from surface heterogeneity and roughness.

The lithium-ion transference number (t_{Li+}) was evaluated using a combination of chronoamperometry and EIS. Chronoamperometric measurements were carried out by applying a constant voltage of 30 mV for 90 min, while EIS was recorded over a frequency range of 100 kHz to 5 mHz. The experiments were conducted on Li||SPE-UV||Li symmetric cells at 40 °C. The t_{Li+} values were then determined following the Bruce–Vincent–Evans method. Ionic conductivity (σ) was determined via EIS. The measurements were carried out using a 20 mV AC sinusoidal voltage over a frequency range of 0.1 Hz–1 MHz. SPE discs, 16 mm in diameter and approximately 150 μm thick, were placed between two stainless-steel blocking electrodes inside an EL-Cell Std (EL-CELL, Germany). To ensure an accurate cell constant, the SPE thickness was precisely measured with a Mitutoyo micrometer before and after each test. The experiments were conducted in a temperature-controlled chamber (MK 53 E2, BINDER, Germany), spanning -10–80 °C. At each temperature, cells were equilibrated for 100 min, and measurements were collected at 10 °C intervals. The ionic conductivity was then calculated using $\sigma = L/(R \times A)$, where L represents the SPE thickness, R is the bulk resistance from EIS, and A is the electrode contact area. The electrochemical stability window (ESW) of the system was probed at 40 °C using a coin-cell in which the SPE was placed between a lithium metal disk and a working electrode (WE) made by blending conductive carbon with PVDF in an 8:2 wt ratio and casting it onto an aluminium current collector. The study employed two approaches: anodic linear sweep voltammetry (LSV), scanning from 3 V (OCV) to 5 V at 0.1 mV s^{-1}, and chronoamperometry, applying a series of stepped potentials within the same 3–5 V range to monitor current response.

3. Results and discussion

3.1. Structural characterization

To gain insight into the crosslinking process, gel content measurements were performed using ethyl acetate (EtOAc), selected based on the known solubility of the constituent polymers. When the crosslinked sample was immersed in EtOAc and subsequently dried to constant weight, 81.4 % of the material remained. The small mass loss observed can be attributed to the extraction of lithium salt, photoinitiator [29], and impurities originating from Re-PVB in the formulation. These findings indicate that the crosslinking process effectively generates covalent linkages between the chains of polymers, thereby retaining a portion of the lithium salt and photoinitiator within the matrix. Repeating the experiment yielded masses of 82.4 % and 81.2 %, consistent with the initial measurement.

To further assess the effectiveness of crosslinking in the SPE-UV electrolyte, photorheological measurements were carried out (Fig. 2a). The sample was exposed to UV irradiation at an intensity of 40 mW cm^{-2}, while subjected to a constant shear rate of 0.1 s^{-1}, within the linear viscoelastic regime. After an initial stabilization period of 30 s, the

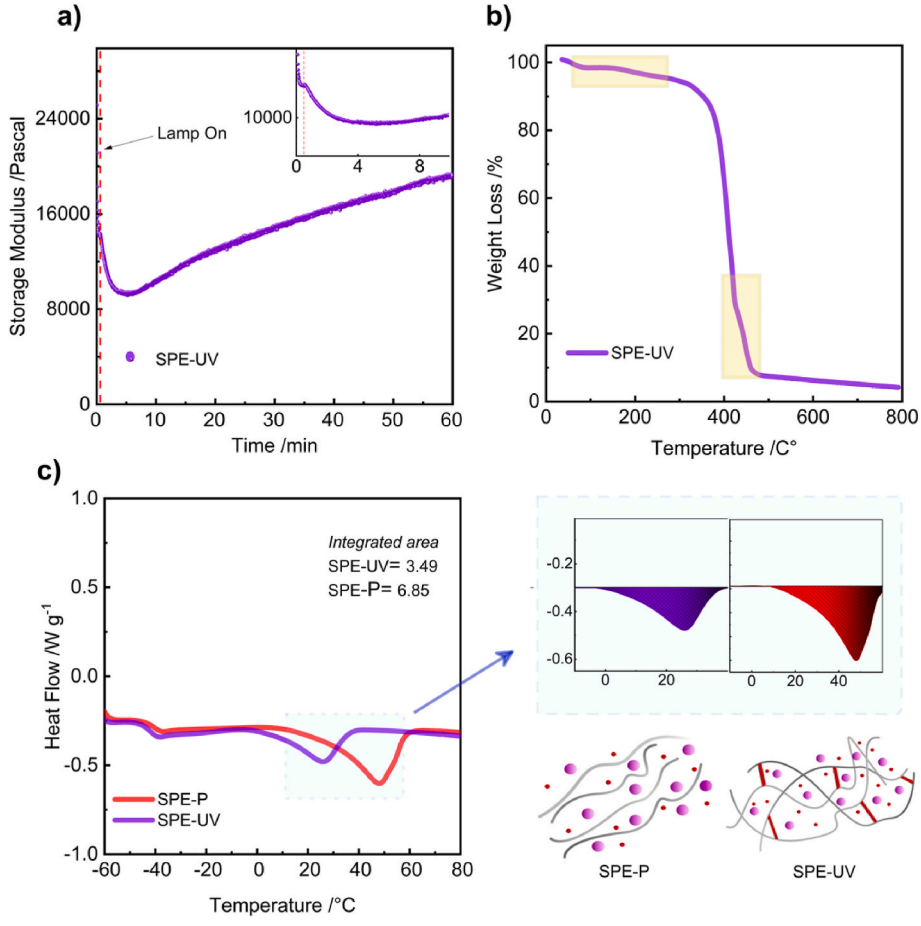

Fig. 2. Photorheology test (a), TGA curves (b), and DSC thermograms (c) of the SPEs under study.

UV source was activated. A small peak in the storage modulus (G′) can be observed, reflecting the onset of localized photopolymerization triggered by 4,4-difluorobenzophenone [30,31]. This is followed by a gradual decrease in G′ at a slowing rate until an inflection point is reached at 4.30 min. Beyond this point, G′ increases again, progressing toward a quasi-linear regime. In this stage, polymerization proceeds at a decelerating rate, hindered by the increasing viscosity of the system [32–34].

Thermogravimetric analysis (TGA) was carried out on the SPE-UV electrolyte, between 30 and 550 °C under nitrogen flow (Fig. 2b), to assess its thermal behavior. The sample remains largely stable until the temperature approaches 350 °C, indicating notable heat resistance comparable to that of the non-crosslinked membrane (SPE-P). Three main degradation steps are detected. The first weight loss, occurring entirely below 200 °C, is minor and corresponds to the release of surface-bound moisture, consistent with the hygroscopic nature of the material [35,36]. A second loss appears between 300 and 350 °C, corresponding to volatilization of plasticizers from the Re-PVB phase and the onset of polymer breakdown. The last stage, occurring above 400 °C, is marked by the conversion of the organic matrix into a carbonaceous residue, which represents the majority of the total mass loss [37,38]. These observations confirm that SPE-UV maintains structural integrity under elevated temperatures, supporting its safe operation in electrochemical devices operating under demanding thermal conditions.

Differential scanning calorimetry (DSC) was employed to evaluate thermal characteristics and phase transitions, particularly focusing on assessing the crystallinity of the SPE electrolytes and their glass transition temperature (T_g). Because crystalline domains hinder ion mobility in SPE, their suppression is crucial for enhancing ionic conductivity [39]. As shown in Fig. 2c, the DSC traces of SPE-P and SPE-UV exhibit melting points (T_m) at 50 °C and 24 °C, respectively. By integrating the peak areas and applying Eq. (2), the crystallinity is estimated to be approximately 22.02 % for SPE-P and 11.04 % for crosslinked SPE-UV. It indicates that crosslinking effectively reduces crystalline domains while simultaneously improving mechanical stability. Furthermore, both samples display a single T_g at −39.9 °C, suggesting a uniform polymer matrix. Overall, the reduced crystallinity and preserved T_g, achieved through Re-PVB incorporation and UV curing, highlight the potential of SPE-UV to provide enhanced ionic conductivity without compromising structural integrity.

3.2. Electrochemical characterization

The lithium-ion transference number (t_{Li}^{+}, viz. the fraction of the total current specifically carried only by Li^+ ions) is a key parameter influencing battery efficiency and performance, where higher values are generally associated with minimized concentration polarization and enhanced power delivery [40]. The chronoamperometry showing current variations to reach the steady state and impedance before and after polarization are shown in Fig. 3a and b, respectively. The SPE-UV exhibits a t_{Li}^{+} of 0.35 at 40 °C, determined using the Bruce–Vincent–Evans method [41]. This value is significantly higher than that of the SPE-P, which reaches only about 0.20 at 65 °C, well in line with standard salt-in-polymer PEO-based SPEs [42]. The enhancement in t_{Li}^{+} can be attributed to the crosslinking bridges between polymer chains and the resulting creation of a structured network, which improves chain interconnectivity and facilitates lithium-ion movement between coordination sites compared to a less structured polymer, while

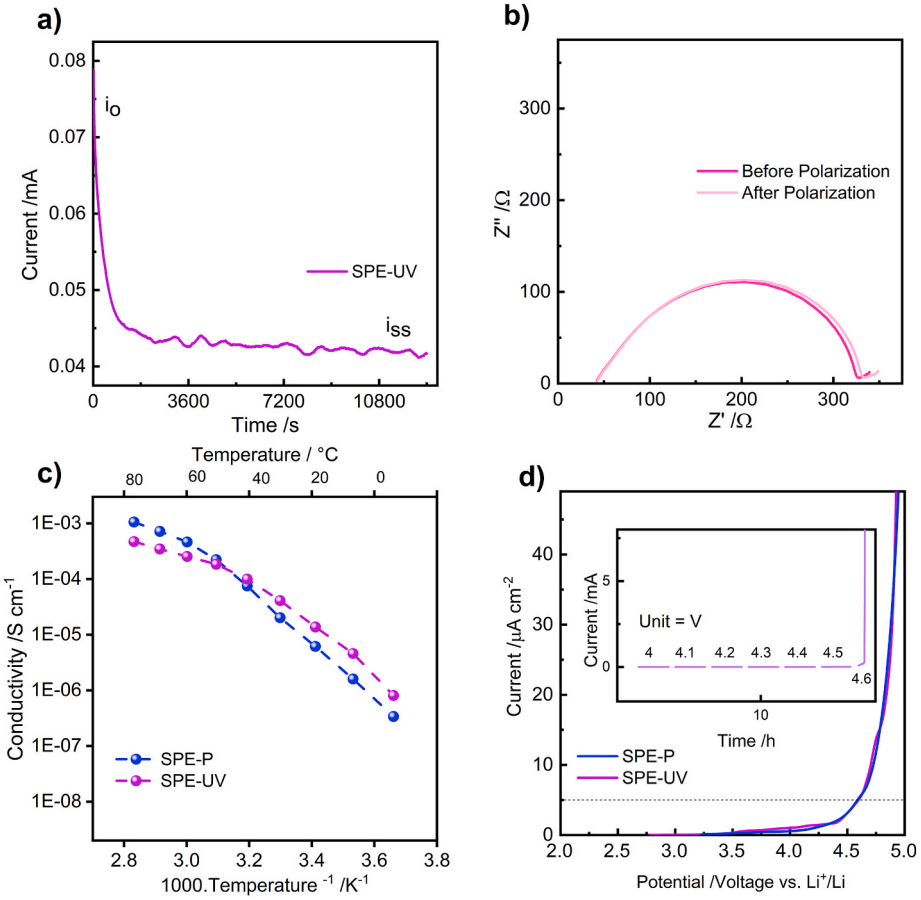

Fig. 3. Chronoamperometry (CA) analysis of Li||SPE-UV||Li under a 30 mV polarization (a). Nyquist plots of Li||SPE-UV||Li before and after polarization (b). Arrhenius plots of ionic conductivity for SPE-UV and SPE-P electrolytes (c). LSV curves of Li||SPE-P ||WE and Li||SPE-UV||WE cells, with the inset showing the CA curves of SPE-UV ((d).

simultaneously restricting anion mobility [43].

The ionic conductivity (σ) of SPE-P and SPE-UV was evaluated by EIS at different temperatures. The Arrhenius plot for both electrolytes in the temperature range of −10 °C–80 °C is shown in Fig. 3c. At elevated temperatures, the σ values of SPE-UV are slightly lower than those of SPE-P. This behavior arises from the reduced chain mobility of the crosslinked SPE-UV, whereas in SPE-P, ion transport is predominantly enhanced by the melting of crystalline domains at high temperatures [29,44,45]. However, below 50 °C, this trend reverses, and SPE-UV exhibits higher σ values. Indeed, UV treatment during membrane preparation induces the formation of new covalent bonds that block PEO structure in its amorphous state even at lower temperatures. These bonds restrict the mobility of PEO chains, preserving the amorphous structure and thereby enhancing ionic transport at low temperature, compared to standard non-crosslinked PEO-LiTFSI systems [46,47].

The electrochemical stability window of the SPEs was investigated to verify their safe operation in solid-state Li-metal batteries [48]. Linear sweep voltammetry (LSV) was employed to identify the anodic decomposition potential, i.e., the voltage at which oxidative breakdown begins. As shown in Fig. 3d, both samples exhibit high oxidative tolerance, with no significant increase in current density up to above 4.5 V, when adopting a cut-off criterion of 5 μA cm^{-2}. To gain further insight into the specific upper voltage limit, chronoamperometric tests were performed on the SPE-UV electrolyte. Constant potential was applied for 1 h intervals at increasingly high voltage steps. The inset of Fig. 3d clearly points out that the current response remains steady for 60 min at 4.5 V, whereas at 4.6 V, a rise in current accompanied by intermittent spikes appears after ~30 min, indicating the beginning of electrolyte degradation.

Based on the enhanced ionic conductivity at lower temperatures and other promising results of SPE-UV, and considering our aim to apply UV curing to SPE-P (which already shows excellent performance at 65 °C), a symmetric Li||SPE-UV||Li cell was assembled to evaluate the effect of UV curing on the behaviour of this truly solid-state electrolyte, particularly performance and related stability upon cycling in battery cells under moderate conditions (40 °C) [29]. Rate capability was evaluated through galvanostatic reversible lithium plating/stripping cycling at successive current densities of 0.02, 0.05, 0.10, and 0.20 mA cm^{-2}, followed by a return to 0.025 mA cm^{-2}. Each step was performed at a fixed plated/stripped areal capacity per half-cycle of 0.20 mAh cm^{-2} to probe the electrolyte capability towards dendrite resistance/suppression, compatibility with Li metal, and sustained operation across varying current regimes (Fig. 4). As shown in Fig. 4a, the SPE-UV cell demonstrates excellent rate capability, maintaining a low overpotential and showing no signs of short-circuiting (negligible Li dendrite growth at 40 °C) even at the highest applied current density of 0.20 mA cm^{-2},

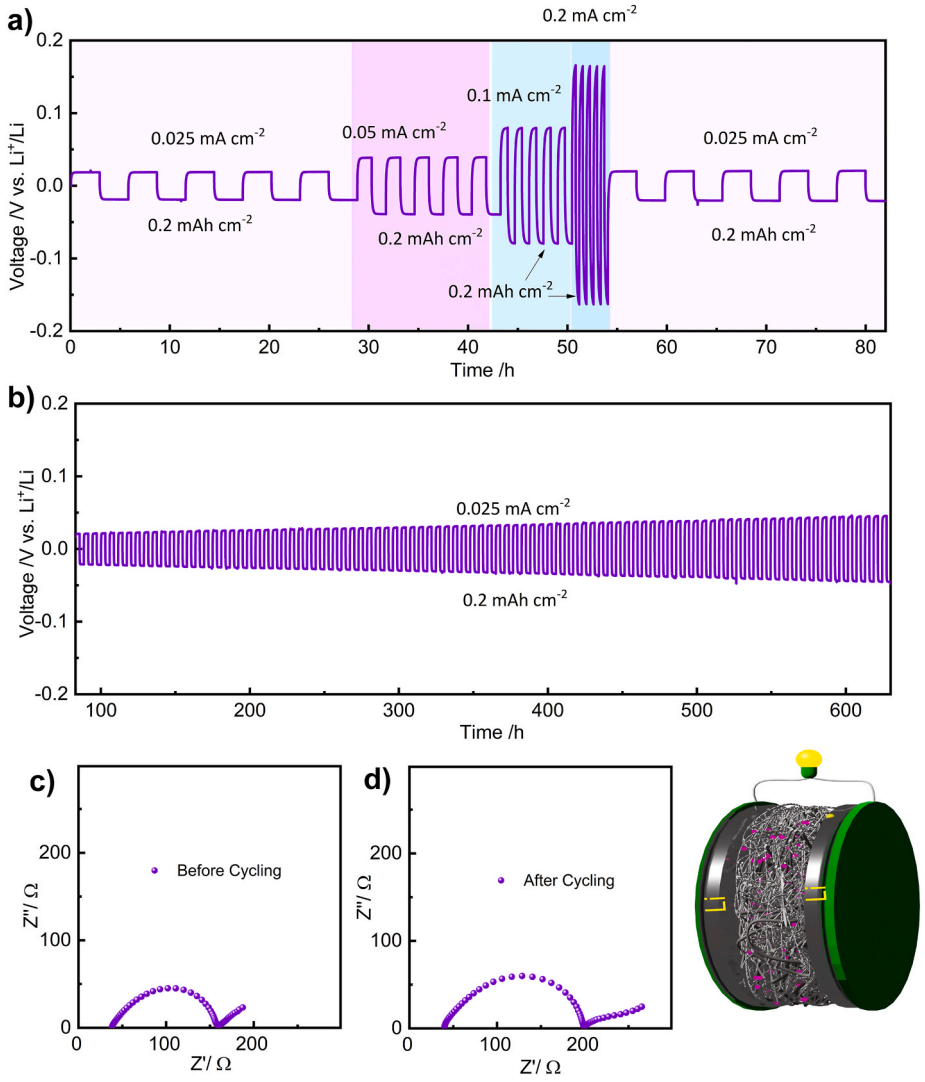

Fig. 4. Galvanostatic Li plating/stripping curves of Li||SPE-UV||Li symmetric cell at 40 °C under 0.025 mA cm^{-2} up to 0.2 mA cm^{-2} (a) and as a function of cycling time at 0.025 mA cm^{-2} (b). Nyquist plots obtained before (c) and after cycling (d).

where the overpotential rises only to ~0.20 V. Long-term cycling at 0.02 mA cm^{-2} results in only a marginal increase in overpotential (from 0.02 V to ~0.04 V) over more than 600 h (Fig. 4b), reflecting remarkable stability. EIS measurements were conducted before and after plating/stripping cycling test (Fig. 4c and d). Before cycling, SPE-UV exhibits a low total resistance (~160 Ω) at 40 °C, outperforming its SPE-P counterpart, which reaches similar resistance values only at 65 °C. The R_e is also notably lower for SPE-UV (45 Ω) compared to SPE-P (65 Ω), despite the reduced testing temperature. After extended cycling, R_e remains largely unchanged, while total resistance increases slightly to ~200 Ω, still below that of the non-crosslinked SPE-P. This moderate rise is attributed to the gradual formation of a passivation layer during early cycles, likely consuming a small fraction of the lithium salt and contributing to minor polarization growth. Thus, the prepared electrolyte demonstrates excellent plating/stripping stability at 40 °C, enabled by the synergistic effect of Re-PVB, which provides mechanical reinforcement, and UV-induced crosslinking, which reduces crystallinity and enhances ionic conductivity at moderate temperatures.

To further evaluate the applicability of SPE-UV in SSLMBs, a Li||SPE-UV||LFP full cell was assembled with LFP in a catholyte configuration at high-mass-loading to impose more stringent testing conditions approaching those of real battery operation (Fig. 5a–d). Rate capability tests were performed upon galvanostatic charge/discharge cycling at 40 °C at current rates of 0.025 C, 0.05 C, 0.10 C, and 0.12 C: specific discharge capacities are provided of approximately 169, 149, 144, and 124 mAh g^{-1}, respectively Fig. 5a. When the rate was returned to 0.025 C, the capacity fully recovers to ~169 mAh g^{-1}, confirming the excellent stability of SPE-UV, as well as its ability to sustain efficient Li^+ transport and stable cycling under stress. The cell exhibits an initial Coulombic efficiency (ICE) of ~95 %, which rapidly stabilizes at ~99.9 % in subsequent cycles. As shown in Fig. 5b, the voltage polarization remains minimal over the full range of applied current densities, including at higher C-rates, underscoring the robust cycling durability of the electrolyte system. These findings demonstrate that, even under challenging conditions of thick cathode loading and moderate operating temperature, the SPE-UV electrolyte delivers solid electrochemical performance. To gain further insight into the interfacial kinetics during cycling, EIS was carried out on the Li||SPE-UV||LFP cell at 40 °C, both prior to and following extended reversible operation. As shown in Fig. 5c, the Nyquist plots reveal that R_s remains essentially unchanged, whereas R_{int} exhibits an increase after cycling. The long-term stability was evaluated in a laboratory-scale Li-metal cell in the Li||SPE-UV||LFP configuration, which was cycled at 0.025C rate and 40 °C (Fig. 5d). The solid-state cell delivers an initial charge capacity close to the theoretical value ~165 mAh g^{-1} with an ICE ~94.7 % (3–4 V vs. Li^+/Li). Remarkably, it shows minimal capacity fading over 40 cycles, maintaining ~156 mAh g^{-1}

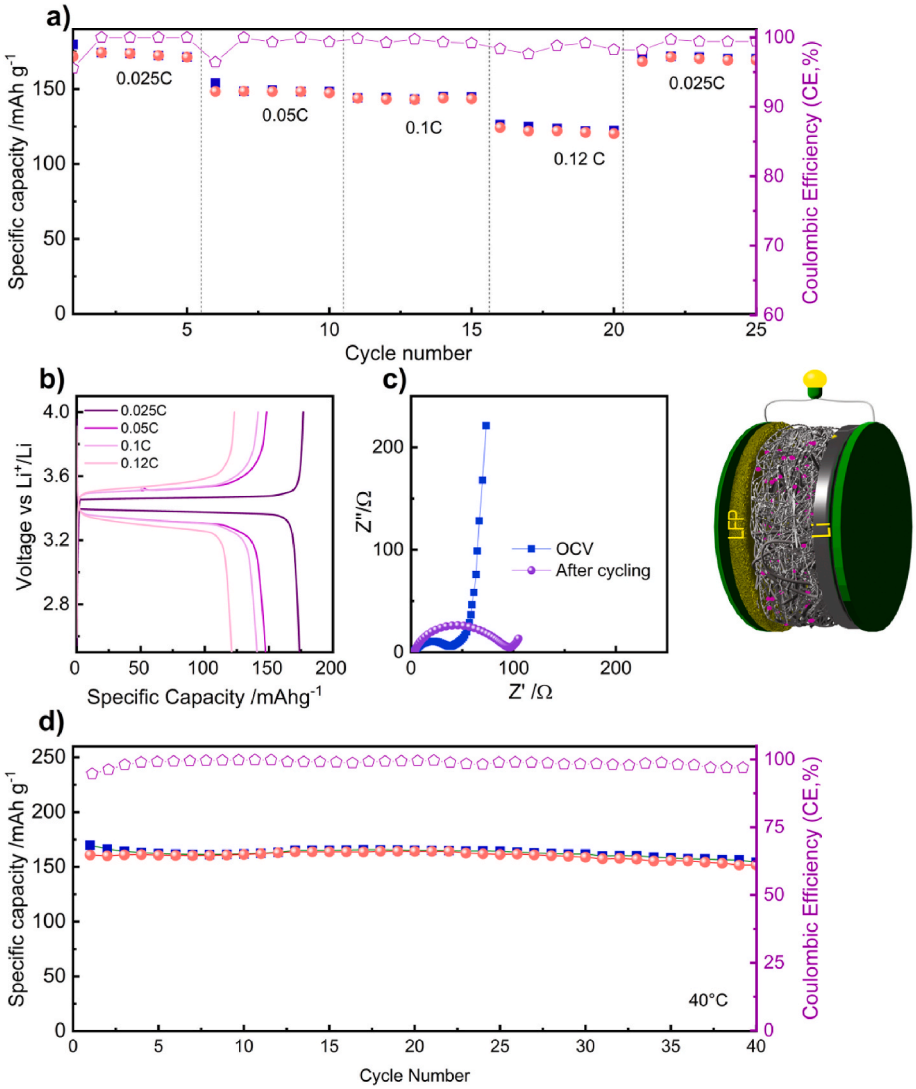

Fig. 5. Rate capability of the Li||SPE-UV||LFP cell at 40 °C (a), with corresponding charge–discharge voltage vs. specific capacity profiles (b), Nyquist plots before and after cycling (c), and cycling performance at 0.025C (d).

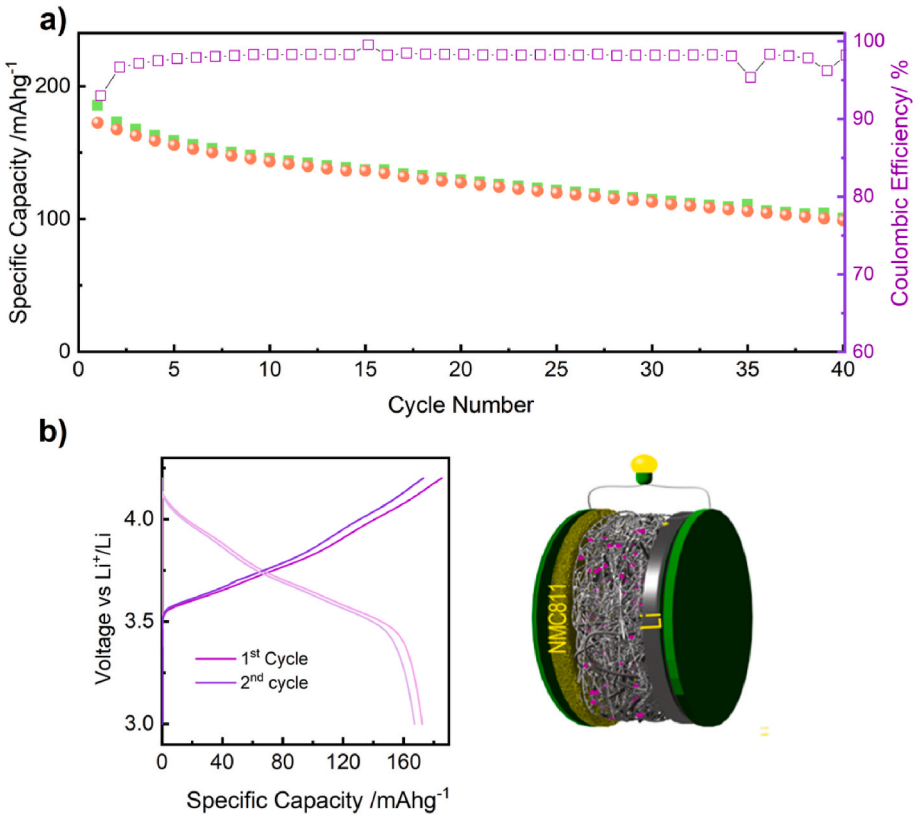

Fig. 6. Cycling performance of the Li||SPE-UV||NMC811 cell at 40 °C (a), with corresponding charge–discharge voltage vs. specific capacity profiles (b).

specific capacity with a CE that rapidly reaches >99 % after the second cycle.

Eventually, based on the promising electrochemical stability results, a Li||SPE-UV||NMC811 full cell was assembled using a high-mass-loading NMC811 catholyte, and E (V) *vs.* Q profiles, as well as the cycling, are shown in Fig. 6a and b. Tests were conducted at 40 °C under challenging conditions to simulate real battery cell operation, which included: the use of NMC811 cathode, which typically experiences rapid capacity fade even with liquid electrolytes at room temperature, and a thick, high-loading electrode, which further promotes degradation. Despite these rigorous conditions, the truly solid crosslinked PEO-PVB electrolyte shows the capability to function in combination with high-energy 4V-cells cathodes, delivering an initial charge capacity of ~180 mAh g^{-1} with an ICE of 92 % at 0.025 C (3–4.2 V *vs.* Li^+/Li). In the second cycle, the capacity stabilizes at 173 mAh g^{-1} with a CE of 96 %, and after 40 cycles, the cell maintains 100 mAh g^{-1} with a CE of 98 %, highlighting the excellent stability and performance of SPE-UV even in demanding SSLMBs at moderately low temperature.

Summarizing, the newly developed safe, sustainable-by-design SPE-UV exhibits promising performance in demanding SSLMBs in combination with medium - LFP or high-voltage - NMC811 cathodes at high active material loading, which is remarkable for a truly solid-state system reversibly operating at moderate temperature. This result arises from the incorporation of re-PVB, which enhances mechanical robustness, combined with UV-induced crosslinking, which reduces crystallinity and increases ionic conductivity, concurrently allowing for a high-performing truly solid polymer electrolyte.

4. Conclusion

The development of high-energy-density, mechanically robust, safe, sustainable-by-design lithium metal cells relies heavily on scalable and environmentally responsible electrolyte technologies, compatible with moderate-temperature processing and readily up-scalable to large-scale production. In this respect, here we highlighted the use of recycled polymers together with a dry, solvent-free, and energy-efficient UV-induced crosslinking process to develop a truly solid-state polymer electrolyte. The electrolyte combined PEO as the ion-conductive phase with mechanically robust Re-PVB obtained by direct recycling of waste PVB used as an interlayer polymer in laminated glasses, forming a crosslinked matrix that provides excellent mechanical stability, Li-metal compatibility, and a wide electrochemical stability window. The material was succesfully demonstrated to operate under moderate conditions (40 °C) and showed promising potential for improving the sustainability, safety, and scalability of lithium metal batteries. Comprehensive electrochemical investigation and testing demonstrated stable, prolonged lithium plating/stripping with low interfacial resistance at relatively low temperature (compared to standard solid-state PEO-LiTFSI salt-in-polymer electrolytes), while full cells containing medium (LFP) or high-V (NMC811) cathodes in high-loading catholyte configurations delivered high specific capacities and robust rate performance. This newly proposed dual-modification strategy showcased a viable route to sustainable, high-performance solid polymer electrolytes, advancing the practical realization of environmentally friendly, efficient SSLMBs.

CRediT authorship contribution statement

Leonardo Balducci: Investigation, Methodology, Validation, Visualization, Writing – original draft. **Hamideh Darjazi:** Investigation, Methodology, Supervision, Validation, Writing – review & editing. **Alessandro Piovano:** Investigation, Methodology, Validation. **Giuseppe Antonio Elia:** Investigation, Methodology, Validation, Visualization. **Claudio Gerbaldi:** Methodology, Supervision, Validation, Writing – review & editing.

Declaration of competing interest

The authors declare that they have no known competing financial interests or personal relationships that could have appeared to influence the work reported in this paper.

Acknowledgements

The SUNRISE project (https://sunrise-project.eu/) has received funding from the European Union's Horizon 2020 Research & Innovation Program under Grant Agreement No 958243. This study was carried out under the National Recovery and Resilience Plan (NRRP), within the MOST – Sustainable Mobility Center and received funding from the European Union Next-GenerationEU (PIANO NAZIONALE DI RIPRESA E RESILIENZA – PNRR Mission 4, Component 2, Investment 1.4 and D.D. 1033 June 17, 2022 of the Ministero dell'Università e della Ricerca (MUR), CN00000023). This manuscript reflects only the authors' views and opinions, neither the European Union nor the European Commission can be considered responsible for them. The authors acknowledge the program Piano Triennale della Ricerca (PTR) within "Ricerca Sistema Elettrico Nazionale 2025–2027″ funded through contributions to research and development by the Italian Ministry of Economic Development. Support under the MUR program "Dipartimenti di Eccellenza 2023–2027" (CUPE17G22001490006) is gratefully acknowledged.

Data availability

Data will be made available on request.

References

[1] T.G. Weldemhret, J.H. Lee, C.U. Park, D.-W. Lee, M.N. Prabhakar, Y.T. Park, J. Il Song, Triboelectric nanogenerator and UV-blocking solid polymer electrolyte nanocomposite from recycled waste cigarette butts, Sustain. Mater. Technol. 39 (2024) e00847, https://doi.org/10.1016/j.susmat.2024.e00847.

[2] H. Darjazi, A. Piovano, G. Meligrana, G.A. Elia, C. Gerbaldi, Using recycled materials in a novel dual binder system for hard carbon anodes: closing the loop toward sustainable Li-/Na-ion batteries, Adv. Funct. Mater. 35 (2025) 2426075, https://doi.org/10.1002/adfm.202426075.

[3] Z. Chen, Y. Zhang, B. Zhu, J. Wang, J. Hu, J. Zou, Z. Jin, X. Li, Y. Zhang, C. Zhang, Construction of high-performance solid-state electrolytes for lithium metal batteries by UV-curing technology, Polym. Test. 132 (2024) 108386, https://doi.org/10.1016/j.polymertesting.2024.108386.

[4] S. Porporato, H. Darjazi, M. Gastaldi, A. Piovano, A. Perez, B. Yécora, A. Fina, G. Meligrana, G.A. Elia, C. Gerbald, On the use of recycled PVB to develop sustainable separators for greener Li-ion batteries, Adv. Sustain. Syst. 9 (2025) 2400569, https://doi.org/10.1002/adsu.202400569.

[5] K.M. Abraham, Z. Jiang, B. Carroll, Highly conductive PEO-like polymer electrolytes, Chem. Mater. 9 (1997) 1978–1988. https://doi.org/10.1021/cm970075a.

[6] Y. Sun, X. Yang, H. Xie, J. Liu, A deep eutectic gel polymer electrolyte prepared by solvent-free UV curing for lithium metal batteries, J. Energy Storage 125 (2025) 117025, https://doi.org/10.1016/j.est.2025.117025.

[7] J. Guo, H. Xu, Y. Sun, K. Chen, X. Zhang, H. Xie, Y. Jiang, J. Liu, Borate-containing triblock copolymer electrolytes for improved lithium-ion transference number and interface stability, J. Colloid Interface Sci. 660 (2024) 565–573, https://doi.org/10.1016/j.jcis.2024.01.097.

[8] Y. Jiang, K. Chen, J. He, Y. Sun, X. Zhang, X. Yang, H. Xie, J. Liu, A self-healing composite solid electrolyte with dynamic three-dimensional inorganic/organic hybrid network for flexible all-solid-state lithium metal batteries, J. Colloid Interface Sci. 678 (2025) 200–209, https://doi.org/10.1016/j.jcis.2024.09.119.

[9] M. Zhou, W. Chen, H. Yang, Y. Hu, T. Lei, D. Chen, S. Wang, Y. Zhang, J. Xiong, Molecular Crowding Solid Polymer Electrolytes for Lithium Metal Battery by In Situ Polymerization, Adv. Energy Mater. 15 (2025) 2403082, https://doi.org/10.1002/aenm.202403082D.

[10] B. Oh, Evaluation and characteristics of a blend polymer for a solid polymer electrolyte, Solid State Ionics 124 (1999) 83–89, https://doi.org/10.1016/S0167-2738(99)00129-0.

[11] Y. Zhang, W. Lu, L. Cong, J. Liu, L. Sun, A. Mauger, C.M. Julien, H. Xie, J. Liu, Cross-linking network based on poly(ethylene oxide): solid polymer electrolyte for room temperature lithium battery, J. Power Sources 420 (2019) 63–72, https://doi.org/10.1016/j.jpowsour.2019.02.090.

[12] T. Sakakibara, M. Kitamura, T. Honma, H. Kohno, T. Uno, M. Kubo, N. Imanishi, Y. Takeda, T. Itoh, Cross-linked polymer electrolyte and its application to lithium polymer battery, Electrochim. Acta 296 (2019) 1018–1026, https://doi.org/10.1016/j.electacta.2018.11.155.

[13] M. Jia, P. Wen, Z. Wang, Y. Zhao, Y. Liu, J. Lin, M. Chen, X. Lin, Fluorinated bifunctional solid polymer electrolyte synthesized under visible light for stable lithium deposition and dendrite-free all-solid-state batteries, Adv. Funct. Mater. 31 (2021) 2101736, https://doi.org/10.1002/adfm.202101736.

[14] Z. Xiao, T. Long, L. Song, Y. Zheng, C. Wang, Research progress of polymer-inorganic filler solid composite electrolyte for lithium-ion batteries, Ionics (Kiel) 28 (2022) 15–26, https://doi.org/10.1007/s11581-021-04340-2.

[15] V.P. Hoang Huy, S. So, J. Hur, Inorganic fillers in composite gel polymer electrolytes for high-performance lithium and non-lithium polymer batteries, Nanomaterials 11 (2021) 614, https://doi.org/10.3390/nano11030614.

[16] L. Hu, X. Gao, H. Wang, Y. Song, Y. Zhu, Z. Tao, B. Yuan, R. Hu, Progress of polymer electrolytes worked in solid-state lithium batteries for wide-temperature application, Small 20 (2024) 2312251, https://doi.org/10.1002/smll.202312251.

[17] E. Wang, Z. Lu, C. Liu, S. Wang, R. Yang, C. Jin, UV curved PESF-LLZTO composite solid electrolyte to in situ construct ultrastable interface for all solid-state lithium battery, J. Electrochem. Soc. 171 (2024) 040544, https://doi.org/10.1149/1945-7111/ad3eb8.

[18] F. Deng, X. Wang, D. He, J. Hu, C. Gong, Y.S. Ye, X. Xie, Z. Xue, Microporous polymer electrolyte based on PVDF/PEO star polymer blends for lithium ion batteries, J. Membr. Sci. 491 (2015) 82–89, https://doi.org/10.1016/j.memsci.2015.05.021.

[19] K.K. Kumar, M. Ravi, Y. Pavani, S. Bhavani, A.K. Sharma, V.V.R. Narasimha Rao, Investigations on PEO/PVP/NaBr complexed polymer blend electrolytes for electrochemical cell applications, J. Membr. Sci. 454 (2014) 200–211, https://doi.org/10.1016/j.memsci.2013.12.022.

[20] S. Rajendran, R. Shanker Babu, M. Usha Rani, Effect of Complexing Salt on Conductivity of PVC/PEO Polymer Blend Electrolytes, Bull. Mater. Sci. 34 (2011) 1525–1530, https://doi.org/10.1007/s12034-011-0354-3.

[21] B.K. Choi, Y.W. Kim, H.K. Shin, Ionic conduction in PEO-PAN blend polymer electrolytes, Electrochim. Acta 45 (2000) 1371-1374, https://doi.org/10.1016/S0013-4686(99)00345-X..

[22] A. Patriarchi, H. Darjazi, A. Piovano, L. Balducci, N. Arcieri, M.Á Muñoz-Márquez Nobili F., C. Gerbaldi, Unlocking sustainable-by-design Li-metal batteries by recycled PVB in blend polymer electrolytes, ChemSusChem (2025) 2501288, https://doi.org/10.1002/cssc.202501288.

[23] F. Zhang, G. Dong, J. Liu, S. Ye, X. Diao, Polyvinyl butyral-based gel polymer electrolyte films for solid-state laminated electrochromic devices, Ionics (Kiel) 23 (2017) 1879–1888, https://doi.org/10.1007/s11581-017-1996-y.

[24] Y. Ren, Y. Yang, J. Zhang, Y. Ma, C. Chen, PVDF/PVB composite polymer electrolyte membranes with high conductivity and excellent cycling performance for lithium-ion batteries, J. Appl. Polym. Sci. 142 (2025) e56459, https://doi.org/10.1002/app.56459.

[25] S. Gopal, S.A. Agnihotry, V.D. Gupta, Ionic Conductivity in Poly(Vinyl Butyral) Based Polymeric Electrolytes: Effect of Solvents and Salts, Sol. Energy Mater. Sol. Cells 44 (1996) 237–250. https://doi.org/10.1016/0927-0248(96)00023-2.

[26] W. Wang, S. Guan, M. Li, J. Zheng, C. Xu, A novel hybrid quasi-solid polymer electrolyte based on porous PVB and modified PEG for electrochromic application, Org. Electron. 56 (2018) 268–275, https://doi.org/10.1016/j.orgel.2018.01.035.

[27] Y. Lu, W. Liao, S. Chen, Water vapor absorption of Polyvinyl Butyral (PVB) interlayer for laminated glass, Construction and Building Materials 478 (2025) 141325. https://doi.org/10.1016/j.conbuildmat.2025.141325.Y.

[28] V. Nikitakos, A.D. Porfyris, K. Beltsios, C. Papaspyrides, S. Bordignon, M. R. Chierotti, S. Nejrotti, M. Bonomo, C. Barolo, A. Piovano, R. Pfaendner, B. Yecora, A. Perez, An integrated characterization strategy on board for recycling of poly(vinyl butyral) (PVB) from laminated glass wastes, Polymers (Basel) 16 (2023) 10, https://doi.org/10.3390/polym16010010.

[29] M. Gastaldi, F. Gambino, H. Darjazi, A. Jouhara, S. Malburet, M. Zanetti, G. Saracco, G.A. Elia, C. Gerbaldi, Dry extrusion of poly(ethylene oxide)-polycarbonate all-solid-state electrolytes for Li-metal batteries: effect of UV-crosslinking on the electrochemical performance, Mater. Today Energy 52 (2025) 101947, https://doi.org/10.1016/j.mtener.2025.101947.

[30] C. Noè, A. Cosola, A. Chiappone, M. Hakkarainen, H. Grützmacher, M. Sangermano, From polysaccharides to UV-curable biorenewable organo/hydrogels for methylene blue removal, Polymer (Guildf.) 235 (2021) 124257, https://doi.org/10.1016/j.polymer.2021.124257.

[31] C. Noè, C. Tonda-Turo, A. Chiappone, M. Sangermano, M. Hakkarainen, Light processable starch hydrogels, Polymers (Basel) 12 (2020) 1359, https://doi.org/10.3390/polym12061359.

[32] A. Rivera-Pousa, J.M. Otero-Mato, H. Montes-Campos, T. Méndez-Morales, D. Diddens, A. Heuer, L.M. Varela, Ternary solid polymer electrolytes at the electrochemical interface: a computational study, Macromolecules 57 (2024) 3921–3936, https://doi.org/10.1021/acs.macromol.3c02669.

[33] R.D. Corder, S.C. Dudick, J.E. Bara, S.A. Khan, Photorheology and gelation during polymerization of coordinated ionic liquids, ACS Appl. Polym. Mater. 2 (2020) 2397–2405, https://doi.org/10.1021/acsapm.0c00343.

[34] E.L. Quirk, M.C. Burroughs, D.J. Mai, In situ Photo-Rheology monitors viscoelastic changes in photo-responsive polymer networks, J. Vis. Exp. 20 (2025) 220, https://doi.org/10.3791/68394.

[35] A. Siu, J. Schmeisser, S. Holdcroft, Effect of water on the low temperature conductivity of polymer electrolytes, J. Phys. Chem. B 110 (2006) 6072–6080, https://doi.org/10.1021/jp0531208.

[36] L. Yan-long, W. Tie-hang, S. Li-jun, Determination of bound water content of loess soils by isothermal adsorption and thermogravimetric analysis, Soil Sci. 180 (2015) 90–96, https://doi.org/10.1097/SS.0000000000000121.

[37] H. Mudila, P. Prasher, H. Kapoor, S. Rana, M.G.H. Zaidi, Electrochemical characterization and HOMO-LUMO studies on fabricated PVB/Graphite and PVB/

GO nanocomposites, Port. Electrochim. Acta 38 (2020) 69–78, https://doi.org/10.4152/pea.202002069.
[38] H. Tang, Y. Su, T. Hu, S. Liu, S. Mu, L. Xiao, Synergetic effect of LaB_6 and ITO nanoparticles on optical properties and thermal stability of poly(vinylbutyral) nanocomposite films, Appl. Phys. A 117 (2014) 2127–2132, https://doi.org/10.1007/s00339-014-8632-8.
[39] H. Darjazi, M. Falco, F. Colò, L. Balducci, G. Piana, F. Bella, G. Meligrana, F. Nobili, G.A. Elia, C. Gerbaldi, Electrolytes for sodium ion batteries: the current transition from liquid to solid and hybrid systems, Adv. Mater. 36 (2024) 2313572, https://doi.org/10.1002/adma.202313572.
[40] R. Bouchet, S. Maria, R. Meziane, A. Aboulaich, L. Lienafa, J.-P. Bonnet, T.N. T. Phan, D. Bertin, D. Gigmes, D. Devaux, R. Denoyel, M. Armand, Single-ion BAB triblock copolymers as highly efficient electrolytes for lithium-metal batteries, Nat. Mater. 12 (2013) 452–457, https://doi.org/10.1038/nmat3602.
[41] P.G. Bruce, J. Evans, C.A. Vincent, Conductivity and transference number measurements on polymer electrolytes, Solid State Ionics 28–30 (1988) 918–922, https://doi.org/10.1016/0167-2738(88)90304-9.
[42] R. Jeanne-Brou, J. Deseure, Trang N.T. Phan, R. Bouchet, D. Devaux, Anisotropic ionic transportproperties in solid PEO based electrolytes, Electrochim. Acta 434 (2022) 141268, https://doi.org/10.1016/j.electacta.2022.141268.
[43] L. Feng, Y. Xu, J. Wu, B. Lin, Semi-interpenetrating polymer network-based gel polymer electrolytes for Li-ion batteries applications, J. Electroanal. Chem. 978 (2025) 118885, https://doi.org/10.1016/j.jelechem.2024.118885.
[44] T. Zhu, X. Hao, Y. Cao, T. Li, Y. Li, W. Wang, Ultraviolet-cured heat-resistant and stretchable gel polymer electrolytes for flexible and safe semi-solid lithium-ion batteries, J. Power Sources 613 (2024) 234944, https://doi.org/10.1016/j.jpowsour.2024.234944.
[45] Y. Zou, Y. He, H. Li, S. Deng, W. Tang, S. Deng, PEO-based electrolyte filled with UV-cured 3D cross-linked polymer network for lithium metal batteries, J. Energy Storage 104 (2024) 114619, https://doi.org/10.1016/j.est.2024.114619.
[46] Z. Gadjourova, Y.G. Andreev, D.P. Tunstall, P.G. Bruce, Ionic conductivity in crystalline polymer electrolytes, Nature 412 (2001) 520–523, https://doi.org/10.1038/35087538.
[47] M. Watanabe, N. Ogata, Ionic conductivity of polymer electrolytes and future applications, Br. Polym. J. 20 (1988) 181–192, https://doi.org/10.1002/pi.4980200304.
[48] J.R. Nair, C. Gerbaldi, G. Meligrana, R. Bongiovanni, S. Bodoardo, N. Penazzi, P. Reale, V. Gentili, UV-cured methacrylic membranes as novel gel–polymer electrolyte for Li-ion batteries, J. Power Sources 178 (2008) 751–757, https://doi.org/10.1016/j.jpowsour.2007.08.004.